Magnetospheres of massive stars

M. Küker[1]

[1]*Leibniz-Institut für Astrophysik Potsdam, Germany*

We study the interaction of line-driven winds from massive stars with the magnetic field rooted in these stars by carrying out numerical simulations using the Nirvana MHD code in 2D in spherical polar coordinates. The code's adaptive mesh refinement feature allows high spatial resolution across the whole simulation box. We study both O and Wolf-Rayet stars for a range of magnetic field strengths from weak to strong as measured by the confinement parameter. For weak fields our simulations show that the initially dipolar field opens up far away from the star and a thin disk-like structure forms in the equatorial plane of the magnetic field. For stronger fields the disk is disrupted close to the stellar surface and closed field lines persist at low latitudes. For very strong fields a pronounced magnetosphere forms where the gas is forced to move along the field lines and eventually falls back to the stellar surface.

1 Introduction

Massive stars lack outer convection zones and are therefore not expected to show magnetic activity as observed on stars on the lower main sequence. Nevertheless, surface magnetic fields have been detected for a number of these stars, often with field strengths of the order 1 kG (Hubrig et al. 2011; Petit et al. 2013). As these objects lose mass through line driven winds, such strong magnetic fields must be expected to have a profound impact on the gas flow in the vicinity of the star. Babel & Montmerle (1997) proposed the Magnetically Confined Wind Shock model to explain the X-ray emission of Bp/Ap stars. In this model the wind is trapped in a dipolar field and channeled towards the equatorial plane where gas flows from both hemispheres collide. For the more massive OB stars with their high mass loss rates the gas can no longer be expected to flow along the field lines far away from the stellar surface. Numerical simulations of θ^1 Ori C by ud-Doula & Owocki (2002) indeed show that the initially dipolar magnetic field opens up except for a region at low latitudes and of limited radial extent, where the field lines remain closed and the gas is trapped and actually falls back towards the star. To characterise the magnetic field strength in terms of the kinetic energy of the gas, ud-Doula & Owocki (2002) define the magnetic confinement parameter,

$$\eta_* = \frac{B_0^2 R_*^2}{4\dot{M}v_\infty} \qquad (1)$$

where B_0 is the magnetic field strength at the poles. For small values of η_* no magnetosphere forms. For $\eta_* = 1$ a disk forms in the equatorial plane of the magnetic field where the gas density is enhanced and the flow speed reduced. For θ^1 Ori C a surface field of $\simeq$ 1kG leads to η_*=10 and the formation of a magnetosphere close to the star while at larger distances the flow structure is similar to the η_*=1 case.

Wolf-Rayet stars are the sources of winds with even higher mass loss rates than OB stars. So far little is known about possible magnetic fields. In this paper we present the first results for WR3. Lacking observational constraints, we show numerical simulations for both weak and strong magnetic fields.

2 Model setup

Our model setup is similar to that of ud-Doula & Owocki (2002). We use the Nirvana MHD code Ziegler (2004) in spherical polar coordinates with adaptive mesh refinement in two dimensions. The simulation box is a spherical shell. The inner boundary represents the stellar surface. The outer boundary does not represent a physical boundary. It is chosen far enough from the star to capture the essential physics of the interaction between magnetic field and wind inside the box. Typical choices are five to ten times the stellar radius, R_*. We choose 10 R_* for θ^1 Ori C and 5 R_* for WR3. The basic mesh is equidistant in both the radial and the meridional directions. We use a resolution of 256x128 cells and allow for five refinement levels, which brings the effective mesh size up to 8192x4096.

We start with a dipolar magnetic field that is aligned with the polar axis of the coordinate system. The velocity is purely radial and follows a β law,

$$v_r = v_\infty \left(1 - \frac{R_*}{r}\right)^\beta \qquad (2)$$

where v_∞ is the terminal velocity and β a parameter of order unity. The density is then chosen to keep the mass flow constant throughout the box, i.e. $\rho = \dot{M}/4\pi r^2 v_r$. The gas is assumed isothermal, with the temperature the same as the effective temperature of the star. We use the line force as derived by Castor et al. (1975) in the parametrisation of ud-Doula & Owocki (2002).

The boundary conditions at the inner boundary keep the radial component of the magnetic field fixed while the meridional field component can vary. Density and radial velocity component are kept fixed while the meridional velocity component can vary. We apply the Nirvana code's built-in treatment of

the symmetry axis and outflow conditions on the outer boundary.

Tab. 1: Stellar and wind parameters used in this paper. The second column lists the units. The B_0 value is for $\eta_* = 10$.

		θ^1 Ori C	WR3
M	$M_\odot$	50	11
L	$L_\odot$	10^6	3.8×10^5
T_{eff}	K	50,000	85,000
R	cm	1.3×10^{12}	2×10^{11}
$\dot{M}$	$M_\odot$/a	2.6×10^{-6}	5×10^{-6}
v_∞	km/s	2,300	2,200
ρ_0	g/cm^3	4.3×10^{-11}	10^{-8}
$\bar{Q}$		500	2000
α		0.6	0.6
B_0	kG	0.95	8.33
β		1	0.8

To verify our setup we reproduce the model of ud-Doula & Owocki (2002) for θ^1 Ori C. We then study the Wolf-Rayet star WR3. The stellar and wind properties of this star have been adopted from Crowther (2007). The model parameters for both cases are summarised in Table 1. We choose the strength of the stellar dipole field such that η_* assumes values of 0.1 (weak field), 1 (intermediate), and 10 (strong field), respectively. For WR 3, this corresponds to polar field strengths of 0.833 kG, 2.6 kG, and 8.33 kG.

3 Results

In the non-magnetic case, it is possible to choose a start configuration that is already close to the steady final solution. The system then evolves through a transient phase before the final solution is reached. After that the system does not change any more. Figure 1 shows these steady solutions for the θ^1 Ori C and WR3 models. They are characterised by a sharp decrease of the density above the stellar surface and a corresponding increase of the gas velocity. At the outer boundary of the simulation box the radial gas velocity is approaching the terminal velocity. The radial velocity profiles are close to β laws as in Eq. 2 except close to the star. Note that despite the similar terminal velocities and mass loss rates the mass density in the θ^1 Ori C model is substantially lower than in the WR3 model because the radius of θ^1 Ori C is larger than that of WR3. The time needed to reach the steady state is essentially the time it takes the wind material to cross the simulation box, about 2×10^5 s for θ^1 Ori C and 2×10^4 s for WR 3. The reason for the shorter time scale

is the smaller radius of WR3 and, consequently, the smaller simulation box.
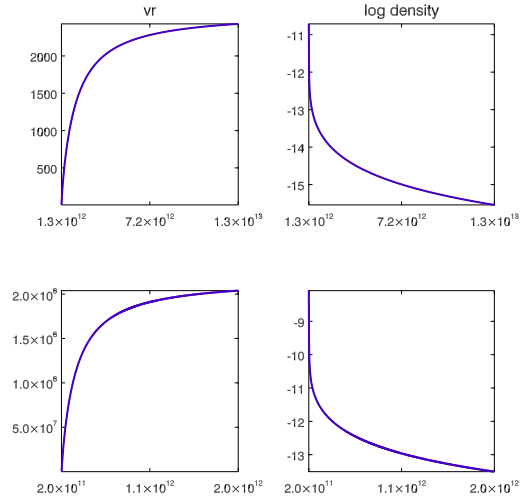
Fig. 1: The non-magnetic solution for θ^1 Ori C (top) and WR3 (bottom). Left: (radial) velocity, right: log(density). Units are km s^{-1} and g cm^{-3}.
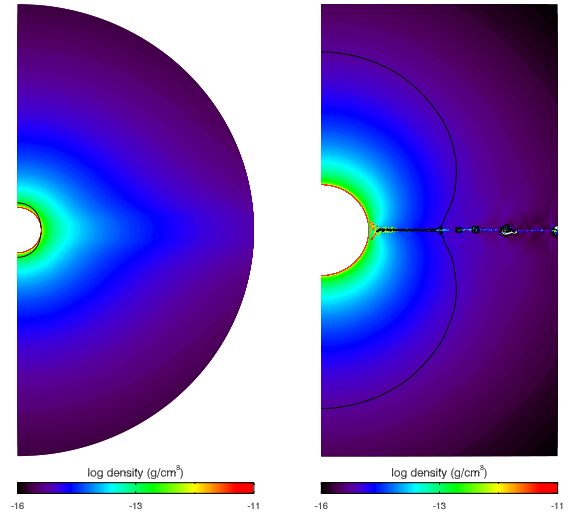
Fig. 2: The density distribution in the inner part of the simulation box for the θ^1 Ori C model with η_*=0.1 (left) and η^*=10 (right). The black line indicates η=1.

For finite field strength there is generally no steady solution. The system settles into a quasi-steady state after about the same time span as in the non-magnetic case but generally remains variable. The amplitude of the variation increases with increasing value of η_*. The variation is very small for η_*=0.1
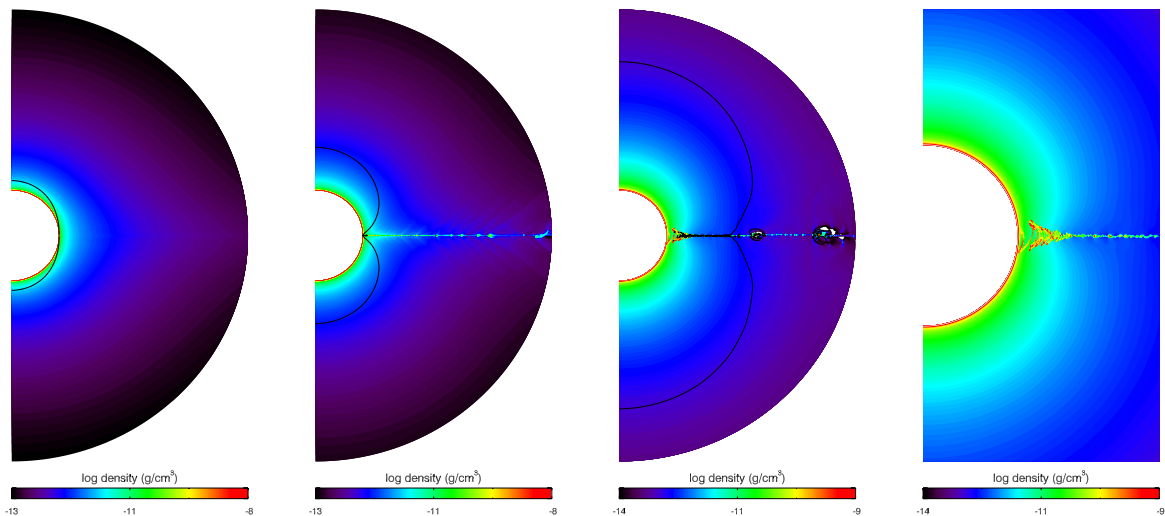
Fig. 3: Density distribution for the WR3 model with η_*= 0.1, 1, and 10 (from left) and a zoom into the inner region for η_*=10 (right panel). The black line indicates η=1.

but substantial for η_*=1 and η_*=10. Total run time is a multiple of the box-crossing time scale, i.e. 10^6 s for θ^1 Ori C and 10^5 s for WR3.

Our model for θ^1 Ori C largely reproduces the results of ud-Doula & Owocki (2002). Figure 2 shows the cases of a weak (η_*=0.1) and strong magnetic field (η_*=10; B_0=0.95 kG). The black line indicates the boundary between the magnetically dominated region and the region dominated by the kinetic energy of the gas, as defined by the ratio of the energy densities,

$$\eta = \frac{B^2/8\pi}{\rho v^2/2}. \tag{3}$$

In the weak field case the magnetically dominated region is limited to a small area right above the stellar surface while in the strong field case the magnetic field is dominant for several stellar radii above the stellar surface.

As in ud Doula & Owocki (2002), the density distribution is oblate for weak magnetic field and prolate for strong magnetic field. For η_*=1 a disk forms in the equatorial plane. The disk is broken up into multiple outwards-moving rings rather than smooth. This is even more pronounced in the strong field case, where we find the same snake-like gas distribution close to the stellar surface at low latitudes as ud-Doula & Owocki (2002).

Figure 3 shows the density distribution for the weak field, intermediate, and strong field cases of the WR3 model. As in case of θ^1 Ori C, the density contours are oblate for weak magnetic field while for intermediate and strong fields the contours are oblate except for the disk in the equatorial plane. Note that the range of density contours in the η_*=10 case is different from the weak field and intermediate cases. The presence of the magnetic field causes a

steeper decrease of the density with radius and the formation of cavities behind the gas rings in the disk. The radial gas velocity shows the opposite behaviour to the density. With increasing field strength there is an increasing contrast between the outflow speeds at high and low latitudes, with the outflow being faster at high latitudes. The mass flux largely follows the density, as the latter varies more strongly with latitude than the gas velocity. Mass flux in the disk is strongly enhanced. The overall mass loss rate is slightly enhanced for weak magnetic field but substantially decreased for strong field.

Our findings for WR3 resemble those for θ^1 Ori C for the same values of the confinement parameter. Note though that the polar field strength of 8.33 kG needed for η_*=10 is very large and may not be realistic. As η_*=1 still requires a polar field strength of 2.6 kG, the weak field case may the most realistic. This would mean no notable variation with time but a pronounced flattening of the density distribution, as in the left panel of Fig. 3.

References

Babel, J. & Montmerle, T. 1997, A&A, 323, 121

Castor, J. I., Abbott, D. C., & Klein, R. I. 1975, ApJ, 195, 157

Crowther, P. A. 2007, ARA&A, 45, 177

Hubrig, S., Schöller, M., Kharchenko, N. V., et al. 2011, A&A, 528, A151

Petit, V., Owocki, S. P., Wade, G. A., et al. 2013, MNRAS, 429, 398

ud-Doula, A. & Owocki, S. P. 2002, ApJ, 576, 413

Ziegler, U. 2004, Journal of Computational Physics, 196, 393

Jorick Vink: For the non-magnetic case, was the instability caused by the LDI (line-driven instability)?

Manfred Küker: Yes.

Andy Pollock: What is the ratio of the mass-loss rate through the disk and through the magnetosphere?

Manfred Küker: The local mass flux in the disk can easily exceed that in the magnetosphere by an order of magnitude, but the disk is too thin to dominate the mass loss. The exact value varies between models and with time, but 25 percent of the total mass-loss rate is a typical value for the region within $\pm 5°$ of the equatorial plane (which makes for 8.7% of the total surface area).

Alex Gormaz-Matemala: How many Gauss does the model have? De la Chevrotière et al. have found an upper limit of only 100 G for WR 6.

Manfred Küker: About 1000 Gauss.